Multi-view interferometric out-of-focus imaging for ice particle characterization

Mohamed Talbi[1], Barbara Delestre[1], Marc Brunel[1,*]

[1]UMR CNRS 6614 CORIA, Department of Physics, University of Normandy, Rouen, France
*corresponding author: marc.brunel@coria.fr, talbim@coria.fr

Abstract A multi-view interferometric particle imaging setup (IPI) is developed and allows the characterization of droplets of liquid water and / or irregular ice particles. The study of these particles highlights first the "signature" of droplets of liquid water during icing. In a second part, using two different angles of views, we perform reconstructions to obtain a 3D description of the rough ice particles, and to estimate the volume of the particles and the possible error rate.

Keywords: Irregular rough particles, Interferometric out-of-focus imaging, Ice crystals, Icing, droplets, 2Dimensional autocorrelation, 2D Fourier transform, Reconstruction, Shapes, Size, Orientation ...

1 Introduction

The study and understanding of icing processes at high altitude receives particular attention, especially for aircraft icing phenomena but also for meteorology and more generally for the characterization of the atmosphere. Interferometric Particle Imaging (IPI) is a measurement technique used for the characterization of triphasic media [1-8]. Indeed, this non-intrusive optical technique allows the measurement of spherical and / or irregular micrometric particles despite a significant distance between the particles and the measuring system (several tens of centimeters). In the case of spherical particles (droplets or bubbles) illuminated by an intense laser beam, the recorded interferogram consists of interference fringes which frequency is inversely proportional to the size of the particle [1-3, 9]. However, for an irregular particle (sand, ash, ice cristal), the recorded interferogram consists of speckle-like pattern. The size of the particle is inversely proportional to the size of the speckle-bean in the speckle-pattern [10-13]. In addition, the use of a multi-views interferometric particle imaging set-up allows to estimate the 3D shape and the orientation of the particle in the measurement field [14, 15]. In summary, this optical technique can be particularly suitable for the study of liquid water droplets and ice crystals suspended in the atmosphere [16]. In situ measurements of these particles beyond the boundary layer surrounding the aircraft in flight seem feasible.

In this study, we will first present the results obtained for the characterization of ice particles using a multi-view IPI setup. Then, we will focus on the particular case of droplets during icing [17]. Finally, in a last part, we will use an analysis procedure for the 3D-reconstruction of possible ice particles whose interferometric images match the patterns recorded with a multi-view IPI setup. Thus, we will be able to estimate the volumes of different possible 3D-objects (ice crystals) which is crucial for Ice Water Content (IWC) estimations, especially for airborne applications.

2 Setup and theoretical background

The experimental setup presented in Fig. 1 includes a cooling chamber, a frequency-doubled Nd:YAG laser emitting 20 mJ, 4 ns pulses at 532 nm, an acquisition system composed of four CCD sensors and numerous optics [15].

The cooling chamber is cylindrical in shape. It is constituted of a double-walled 340l stainless steel column, an insulation layer composed of polyisocyanurate (density 40 kg · m−1), and seven thermocouples to record the temperature at different heights inside the column. The cooling of the latter is ensured by thermofluid circulating in our double wall (the temperature inside the column is about −45°C.). Cold water droplets (around 0°C) of random size (in the range [10 μm; 400 μm]) are sprayed at the top of the column. They fall inside the cooling chamber and freeze.

At the bottom of the column, four BK7 windows are positioned at different angles (0°, +135°, +180°, and −135°) as shown in Fig. 1. The window at 0° enables the entrance of the laser sheet inside the cooled column

and the illumination of the ice particles under free fall. Light scattered by the ice particles is collected through the two windows at ± 135°, offering two perpendicular angles of view. For each angle of view, by using beam splitters, we simultaneously record two images of the same particles: in-focus images [sensors 1 and 3 in Fig. 1(b)] and the corresponding out-of-focus images [sensors 2 and 4 in Fig. 1(b)]. In-focus images are obtained by using far-field objectives provided by ISCOOPTIC (fields of view: 2.45 mm × 2.45 mm, depth of field: 1 mm). Out-of-focus systems consist of Nikon objectives (focus length of 180 mm) with an extension tube providing out-of-focus imaging. The four CCD sensors are synchronized on the laser pulse for a simultaneous acquisition of ice particle images according to both angles of view. In summary, the setup enables us to record two out-of-focus images from two perpendicular views (at ± 135°) as well as the corresponding two in-focus images. For more clarity, we have fixed the reference frame (x, y, z) as presented in Fig. 1. After 2D Fourier transforms of the different interferometric images, the corresponding coordinates in the spectral domain will be denoted (u, v, w). The dimensions of the CCD sensors used for in-focus imaging are 2048 × 2048 pixels (pixel size: 5.5 μm). The dimensions of the CCD sensors used for out-of-focus imaging are 1920 × 1200 pixels (pixel size: 5.86 μm).
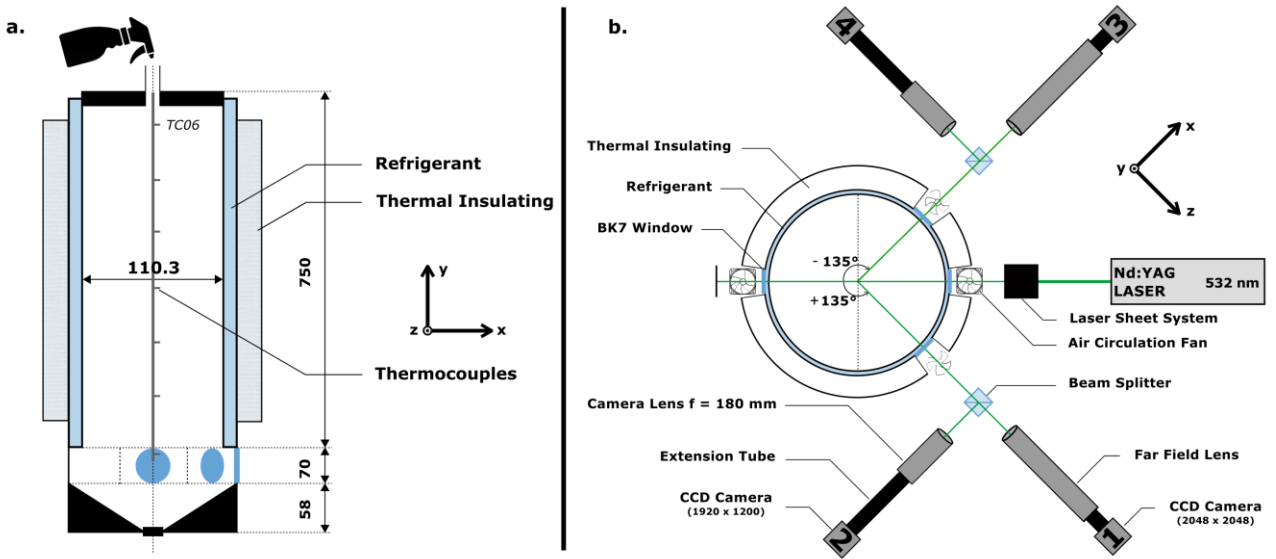

Fig. 1 Experimental setup, (a) side view (dimensions in millimeters), (b) top view.

Unlike the Lorenz-Mie Theory (LMT) which allows to describe rigorously the scattering of a coherent light by a spherical particle, there is no rigorous model in the case of an irregular particle of any shape. However, recent interferometric imaging experiments have validated a simplified approach: it consists in assimilating an irregular particle illuminated by a laser source to a set of point emitters located on its envelope. A scalar expression of the electric field received by the camera can then be obtained. It has been shown that the 2D-autocorrelation of the contour of the projected shape of the particle in the CCD sensor's plane is related to the 2D Fourier transform of its interferometric out-of-focus image. This can be described by the following relationship [18]:

$$|A_{2D}[G_0](dx, dy)| \propto |FT_{2D}[I](\lambda B_{tot} u, \lambda B_{tot} v)| \qquad (1)$$

where I is the intensity of the out-of-focus pattern of the particle and G_0 the electric field emitted by the illuminated particle, λ the wavelength of the laser and B_{tot} the coefficient of the total transfer matrix of all the elements separating the particle and the CCD sensor. For our experimental setup, B_{tot}= -0,0229 m.

We will show that relation (1) is verified for both angles of IPI views in the case of ice particles. Equation (1) will remain verified also for liquid water droplets during their icing transient process. Thus, we will highlight the "signature" of liquid water droplets during icing from the observation of 2D-Fourier transform of IPI images. Finally, from equation (1), we will develop an analysis procedure for the 3D-reconstruction of possible particles whose interferometric images can match the experimental ones recorded using the multi-view IPI

setup. Thus, we will be able to estimate the volumes of the ice particles under observation.

3 Interferometric imaging of ice particles and freezing droplets

Let us first present some experimental results obtained for irregular ice particles using our multi-view setup [15]. Figures 2(a) and 2(b) show the in-focus images recorded from both angles of view (Sensors 1 and 3 in Fig. 1). The size scale is not the exact scale of the CCD sensor. It has been divided by the magnification factor introduced by the in-focus imaging system. This magnification factor has been measured with a calibrated target inserted into the freezing column: it equals - 4.6. The axes of Figs. 2(a) and 2(b) give thus the exact dimensions of the scattering particles. The ice particle has a size of 245 ± 33 μm along the x axis, 265 ± 33 μm along the y axis, and 240 ± 33 μm along the z axis. Figures 2(c) and 2(d) show the two-dimensional autocorrelations of the in-focus images of Figs. 2(a) and 2(b), respectively.
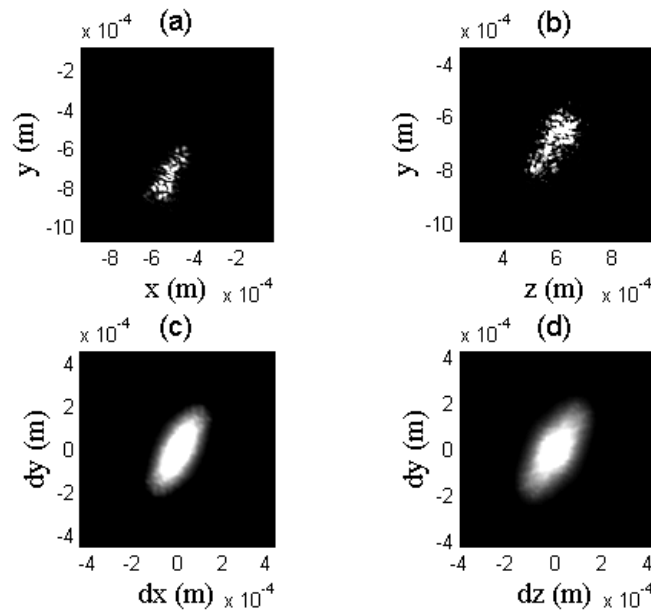

Fig. 2 In-focus images of an ice particle observed with (a) sensor 1 and (b) sensor 3; two-dimensional autocorrelations of the in-focus particle observed (c) in (a) and (d) in (b).

Figures 3(a) and 3(b) show the out-of-focus images recorded simultaneously from both angles of view (with sensors 2 and 4 in Fig. 1). Figures 3(c) and 3(d) present the 2D Fourier transforms of the out-of-focus images of Figs. 3(a) and 3(b), respectively. We can see that for both angles of view, the correspondence between the two-dimensional autocorrelations of the in-focus images [Figs. 2(c) and 2(d)] with the corresponding 2D Fourier transforms of the speckle-like patterns [presented in Figs. 3(c) and 3(d)] is very good in size and shape (the slight differences are due to the binarisation threshold). Equation (1) appears acceptable to compare the contours of both functions in the case of irregular ice particles.
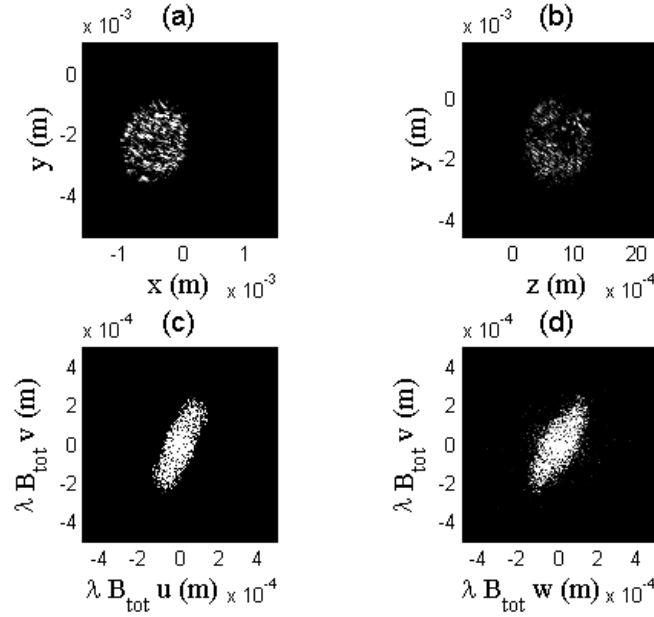
Fig. 3 Out-of-focus images of an ice particle observed with (a) sensor 2 and (b) sensor 4; 2D Fourier transforms of the patterns observed (c) in (a) and (d) in (b).

Let us now look at liquid water droplets during their transient icing process resulting from the very low temperature within the cooling column [17]. Figure 4 shows an example of this specific case. Figures 4(a) and 4(b) show the in-focus images recorded from both angles of view (Sensors 1 and 3 in Fig. 1). For each view, we observe the presence of two bright domains (around the position of the two glare points of a pure liquid droplet) composed of "secondary" light spots more or less separated in space. It appears as if the initial glare points of the droplet had been broken in a large number of secondary emitters, due to the partial solidification of the droplet. Figures 4(c) and 4(d) show the two-dimensional autocorrelations of the in-focus images of Figs. 4(a) and 4(b), respectively.
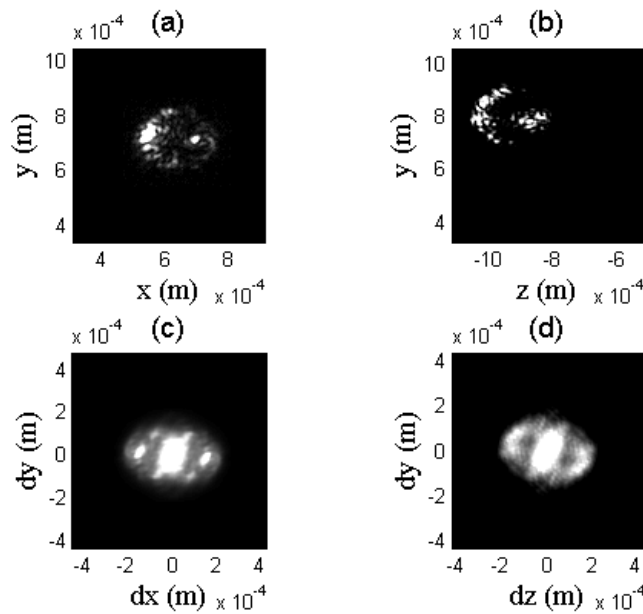

Fig. 4 In-focus images of a freezing droplet observed with (a) sensor 1 and (b) sensor 3; two-dimensional autocorrelations of the in-focus freezing droplet observed (c) in (a) and (d) in (b).

Figures 5(a) and 5(b) show then the interferometric out-of-focus images recorded simultaneously from both

angles of view (with sensors 2 and 4 in Fig. 1). Figures 5(c) and 5(d) represent the 2D Fourier transforms of these out-of-focus images of Figs. 5(a) and 5(b), respectively. We can see that for both angles of view, even if the droplet is icing, the correspondence between the two-dimensional autocorrelations of the in-focus images [Figs. 4(c) and 4(d)] with the 2D Fourier transforms of the speckle-like patterns [presented in Figs. 5(c) and 5(d)] is very good in size and shape. Equation (1) appears acceptable despite the phase change (liquid / solid state).
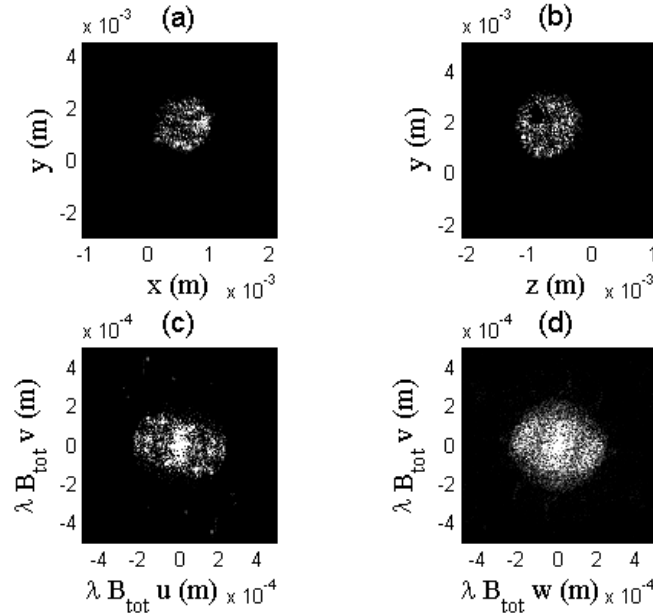

Fig. 5 Out-of-focus images of a freezing droplet observed with (a) sensor 2 and (b) sensor 4; 2D Fourier transforms of the patterns observed (c) in (a) and (d) in (b).

4 3D-reconstructions of ice particles

In the previous section, we have noted that relation (1) is acceptable for ice particles: the contour of the 2D-Fourier transform of the out-of-focus image can thus be likened to the contour of the 2D-autocorrelation of the particle itself. Unfortunately, the 2D-autocorrelation of an object does not give the object itself. Methods exist to predict possible objects whose 2D-autocorrelation match an expected one [19]. One of them is the tri-intersection method that will be used in what follows [19]. Fig. 7(a) shows the 2D-autocorrelation of an initial 2D-shape that would be observed from a first angle of view. Using the tri-intersection method, figures 7(b-g) show 6 possible shapes whose 2D-autocorrelations match Fig. 7(a). Let us assume that Fig. 7(a) corresponds to the 2D-autocorrelation of the projection of a 3D-object according to a first angle of view (set-up of figure 1). This 3D-object can be observed from a second perpendicular angle of view (as in the set-up of figure 1). In the case of an irregularly-shaped object, the projection of the shape of this object according to this second angle of view will be different. It is assumed for example that Fig. 8(a) shows now the 2D-autocorrelation of the initial 2D-shape of the same object when it is observed from a second perpendicular angle of view. Using the tri-intersection method again, figures 8(b-g) show 6 possible shapes whose 2D-autocorrelations match Fig. 8(a).

In practice, for each ice particle, the set-up of figure 1 delivers two interferometric images whose 2D-Fourier transforms are analyzed as those simulated in Fig. 7(a) and 8(a). Combining 6 possible shapes from view 1, with 6 possible shapes from view 2, it is possible to reconstruct 36 possible 3D-objects that match the initial pair of interferometric patterns. We perform a numerical reconstruction by the projection along axis z of one of the possible shapes for view 1 (axes (x,y), shapes of Fig. 7(b-g)), combined with the projection along axis x of one of the possible shapes for view 2 (axes (z,y), shapes of Fig. 8(b-g)). There are 36 possible combinations for 36 possible reconstructed 3D-objects. As the Ice Water Content is a key parameter in atmospheric studies, the volume of all possible reconstructed objects will be compared. The 36 values obtained are thus reported on Fig. 9. It is first important to note that all volumes are in the same range of numerical values. Some volume estimations are clearly lower: they correspond actually to the combination of the 2D-

shapes of Fig. 7(b) or (7g) with the 2D-shapes of Fig 8(b) or 8(g): it means that the particle's volume estimation can suffer bigger error if the particle has sharp ends. But in most experimental cases where particles have curved extremities, it appears that the error in particle's volume estimation remains relatively low, although we can not predict the exact 3D-shape of the object from a pair of interferometric patterns. Similar reconstructions can be performed from experimental patterns to estimate the volume of real ice particles generated in a freezing column. After comparing with the in-focus images recorded simultaneously, our experimental results show that the relative error in particle's volume estimation can reach $\Delta V/_V \approx 30\%$ depending on the choice of the 3D-shape reconstruction.
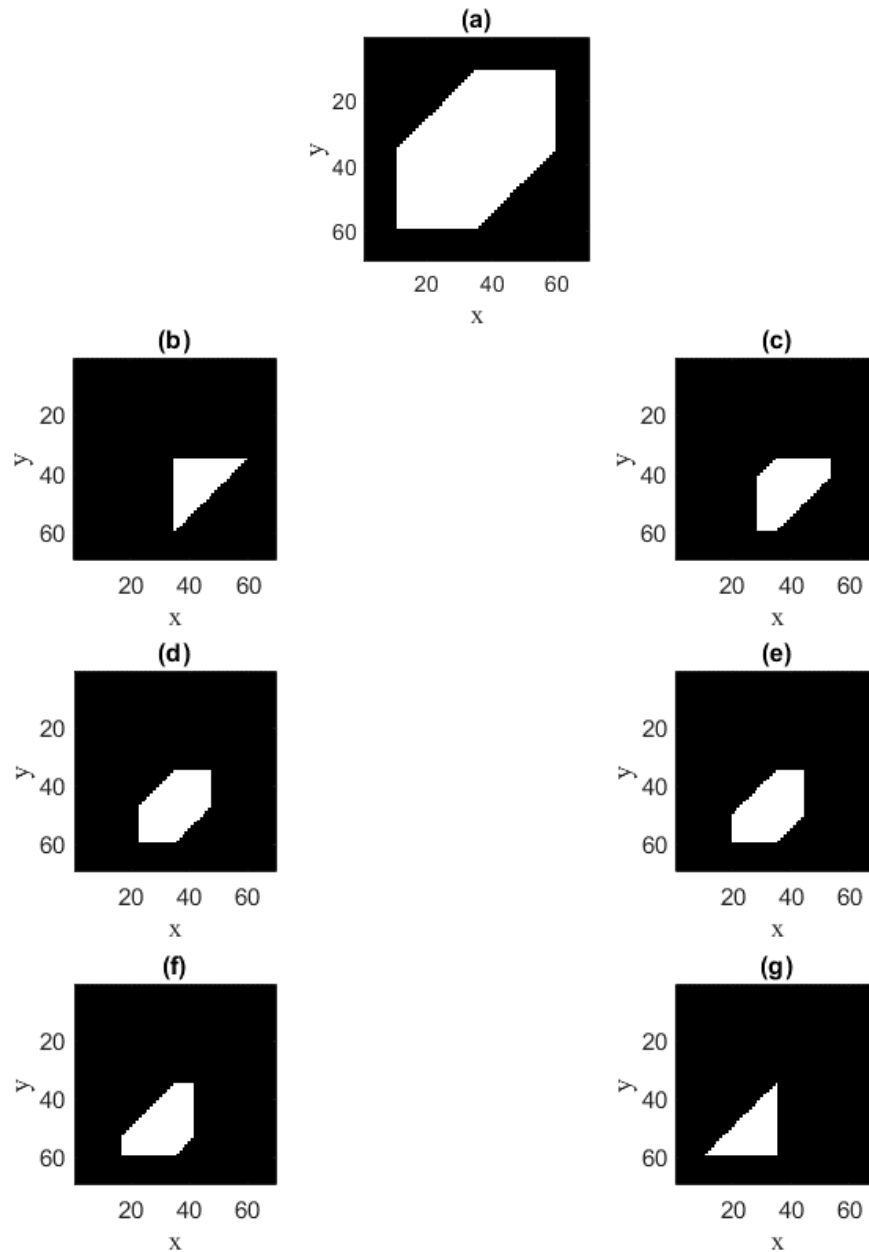

Fig. 7 2D-autocorrelation of an initial 2D-shape (a), and 6 possible 2D-objects whose 2D-autocorrelation is the one of Fig. (a) (b-g) (units in pixels); corresponding to a first angle of view.
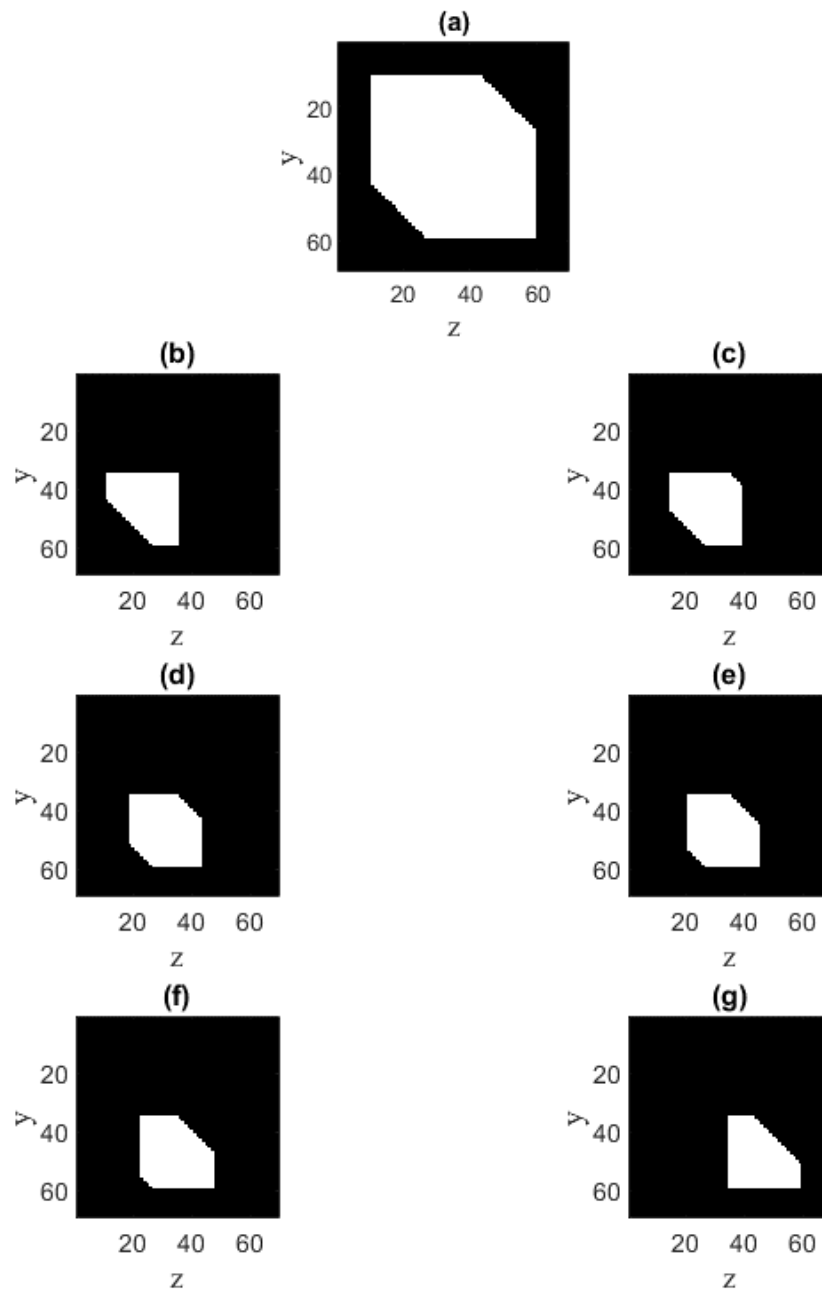
.

Fig. 8 2D-autocorrelation of an initial 2D-shape (a), and 6 possible 2D-objects whose 2D-autocorrelation is the one of Fig. (a) (b-g) (units in pixels); corresponding to a second perpendicular angle of view.
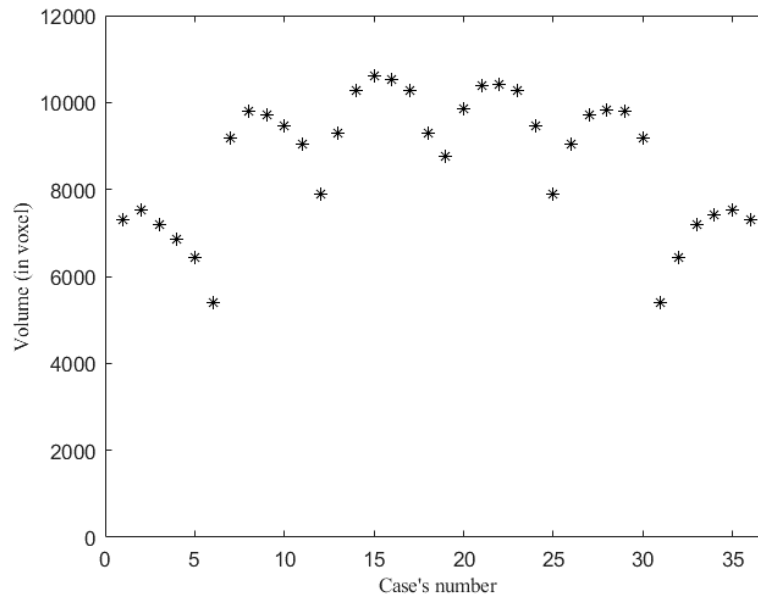
Figure 9. 36 volume's estimations for 36 possible combinations.

5 Conclusion

In this study, we have confirmed that the contour of the projected shape of the particle is related to the 2D Fourier transform of its interferometric out-of-focus image (equation (1) remains acceptable) for liquid water droplets during icing. From the 2D-Fourier transform of the out-of-focus images, we have highlighted some characteristic "signatures" of the phenomenon of icing. IPI can be used to detect and analyze transient phases of this complex phenomenon. For irregular ice crystals, equation (1) is also satisfactory and the contour of the 2D-Fourier transform of the out-of-focus images can be likened to the contour of the 2D-autocorrelation of the particle itself. Finally, we have developed an automated program that delivers possible 2D-shapes of a 2D-object whose 2D-autocorrelation is deduced from the 2D-Fourier transform of interferometric patterns recorded experimentally. Thus, with our multi-view interferometric out-of-focus imaging setup, we are able to reconstruct possible 3D shapes of irregular ice crystals from their experimental out-of-focus images. The volume of the particle and its uncertainty can then be estimated, which could have significant applications for aircraft safety.

References

[1] G. König, K. Anders, and A. Frohn, "A new light-scattering technique to measure the diameter of periodically generated moving droplets," J. Aerosol Sci. 17, 157–167 (1986).

[2] A. R. Glover, S. M. Skippon, and R. D. Boyle, "Interferometric laser imaging for droplet sizing: a method for droplet-size measurement in sparse spray systems," Appl. Opt. 34, 8409–8421 (1995).

[3] T. Kawaguchi, Y. Akasaka, and M. Maeda, "Size measurements of droplets and bubbles by advanced interferometric laser imaging technique," Meas. Sci. Technol. 13, 308–316 (2002).

[4] N. Damaschke, H. Nobach, and C. Tropea, "Optical limits of particle concentration for multi-dimensional particle sizing techniques in fluid mechanics," Exp. Fluids 32, 143–152 (2002).

[5] S. Dehaeck and J. P. A. P. Van Beeck, "Designing a maximum precision interferometric particle imaging set-up," Exp. Fluids 42, 767–781 (2007).

[6] H. Zhang, M. Zhai, J. Sun, Y. Zhou, D. Jia, T. Liu, and Y. Zhang, "Discrimination between spheres and spheroids in a detection system for single particles based on polarization characteristics," J. Quantum Spectrosc. Radiat. Transfer 187, 62–75 (2017).

[7] Z. Ulanowski, E. Hirst, P. H. Kaye, and R. S. Greenaway, "Retrieving the size of particles with rough and complex surfaces from two-dimensional scattering patterns," J. Quantum Spectrosc. Radiat. Transfer 113, 2457–2464 (2012).

[8] M. Brunel, H. Shen, S. Coëtmellec, G. Gréhan, and T. Delobel, "Determination of the size of irregular particles using interferometric out-of-focus imaging," Int. J. Opt. 2014, 143904 (2014).

[9] L. Ouldarbi, G. Pérret, P. Lemaitre, E. Porcheron, S. Coëtmellec, G. Gréhan, D. Lebrun, and M. Brunel, "Simultaneous 3D location and size measurement of bubbles and sand particles in a flow using interferometric particle imaging," Applied optics, 54(25), 7773-7780 (2015).

[10] Z. Ulanowski, P. H. Kaye, E. Hirst, R. S. Greenaway, R. J. Cotton, E. Hesse, and C. T. Collier, "Incidence of rough and irregular atmospheric ice particles from Small Ice Detector 3 measurements,"Atmos. Chem. Phys. 14, 1649–1662 (2014).

[11] P. García Carrascal, S. González Ruiz, and J. P. A. J. Van Beeck, "Irregular particle sizing using speckle pattern for continuous wave laser applications," Exp. Fluids 55, 1851 (2014).

[12] J. Jacquot-Kielar, P. Lemaitre, C. Gobin, Y. Wu, E. Porcheron, S. Coetmellec, G. Gréhan, and M. Brunel, "Simultaneous interferometric in-focus and out-of-focus imaging of ice crystals," Opt. Commun. 372, 185–195 (2016).

[13] M. Brunel, H. Shen, S. Coëtmellec, G. Gréhan, and T. Delobel, "Determination of the size of irregular particles using interferometric out-of-focus imaging," Int. J. Opt. 2014, 143904 (2014).

[14] L. Ouldarbi, M. Talbi, S. Coëtmellec, D. Lebrun, G. Gréhan, G. Perret, and M. Brunel, "3D-shape recognition and size measurement of irregular rough particles using multi-views interferometric out-of-focus imaging," Appl. Opt. 55, 9154–9159 (2016).

[15] M. Talbi, G. Grehan, and M. Brunel, "Interferometric particle imaging of ice particles using a multi-view optical system," Applied optics, 57(21), 6188-6197 (2018)..

[16] E. Porcheron, P. Lemaitre, J. P. A. J. Van Beeck, R. Vetrano, M. Brunel, G. Grehan, and L. Guiraud, "Development of a spectrometer for airborne measurement of droplet sizes in clouds," Journal of the European Optical Society-Rapid publications, 10 (2015).

[17] M. Brunel, M. Talbi, S. Coetmellec, G. Grehan, Y. Wu, J. Jacquot-Kielar, "Interferometric out-of-focus imaging of freezing droplets," Optics Communications, 433, 173-182 (2019).

[18] M. Brunel, S. González Ruiz, J. Jacquot, J. van Beeck, "On the morphology of irregular rough particles from the analysis of speckle-like interferometric out-offocus images," Opt. Commun. 338, 193–198 (2015).

[19] J.R. Fienup, T.R. Crimmins and W. Holsztynski, "Reconstruction of the support of an object from the support of its autocorrelation," J. Opt. Soc. Am. **7**, 3-13 (1982).